DOI: 10.13009/EUCASS2019-159

DOI:

A blade configuration study of vertical axis wind turbines using a CFD approach

Tiantian Zhang[a,b], Zhenguo Wang[a], Wei Huang[a], Derek Ingham[b], Lin Ma[b], Mohamed Pourkashanian[b]*
[a]Department of Aerospace Science and Engineering, National University of Defense Technology
Changsha, Hunan, 410073, P. R. China
[b]Energy 2050, Department of Mechanical Engineering, The University of Sheffield
Sheffield, S3 7RD, the UK
*Corresponding author, Email: lin.ma@sheffield.ac.uk

Abstract

Vertical axis wind turbines (VAWTs) have been attracting increasing attention in recent years in order to save fossil resources and protect the environment. However, the relatively low efficiency of VAWTs has limited their development. This paper studies the influence of the airfoil's maximum camber as well as its position on the performance of the VAWT based on the CFD analysis. During this process, the Kriging model is applied to the samples accessed by the Latin Hypercube Sampling approach. The influence of the airfoil's thickness is studied based on the two-dimensional symmetrical NACA 4 digital airfoils. In addition, the three-dimensional rotating process of the VAWT is studied by simulating a single blade with the assistant of a UDF file. Based on this approach, this paper investigates the 3D blade's shape on its aerodynamic performance and power coefficient. The current result shows that the straight blade with a symmetrical airfoil has the best power efficiency. The thickness of the NACA0018 is the most suitable for the operating conditions investigated.

1. Introduction

Wind turbines are becoming increasingly popular in many countries nowadays. Its main merits are protecting the environment and saving resources and it provides a promising future in the energy field. Vertical axis wind turbines(VAWTs) are effective for small-scale electricity generation and they are also suitable for the urban areas where there are high turbulent wind conditions. They cost less than traditional horizontal axis wind turbines (HAWTs) in that they do not need a yaw control system to actively orient to the direction of the wind.[1] In addition, the gearbox and the generator of the VAWTs are mounted at the bottom of the rotor so that it is easier to install and maintain these devices.[13] The Darrieus type VAWTs are an important type of VAWTs and they are lift based turbines. This paper mainly focuses on this kind of VAWT.

The main reason why VAWT's development is limited is its relatively low efficiency in generating electricity.[1] Various works have been done to study different problems related to the VAWT. For example, the pitching operation, the roughness of the rotor surface, the transition model, the thickness and the curvature of the blade, the tip speed ratio (TSR), etc.[18] With the development of computational fluid dynamics (CFD), numerical studies of the VAWT's rotor has become increasingly popular and attractive because it costs less to simulate the VAWT's rotation than to conduct wind tunnel experiments. Based on the CFD approach, two dimensional (2D) simulations are commonly used nowadays because the commonly used straight blade has the same profile along the spanwise direction. Lanzafame et al.[9] established the 2D unsteady CFD model of the Darrieus VAWT using a sliding mesh method and the results attained match well with the available experimental data. This reflects that a good modeling strategy can make the CFD results convincing. Brusca et al.[4] studied how the rotor's aspect ratio, which is defined as the ratio between blade height and rotor radius, influences the performance of the VAWT and they found that a small aspect ratio can increase the Reynold number and thus improve the power coefficient. The profile of the blade is commonly studied based on the 2D simulation approach. Shukla et al.[15]studied the performance of VAWTs with the blade airfoils of NACA0018, NACA0021, and NACA0025. The results show that the moment coefficients and the power coefficients increase with the increment of the tip speed ratio and NACA0025 has the best performance when the TSR is the same. Chen et al.[5] used the orthogonal algorithm combined automatic CFD approach to study the influence of thickness as well as the thickness's location on the performance of the VAWT. They concluded that the thickness-to-camber ratio is

DOI: 10.13009/EUCASS2019-159

a very important factor in influencing the VAWT's performance. Apart from the symmetrical airfoils, Rainbird et al.[3] confirmed that the virtual camber effect on the airfoil of the VAWT has a significant influence on the performance of the VAWT. Jafaryar et al.[7] studied the influence of the airfoil's shape on the performance of the VAWT and optimized the airfoil based on the RSM and central composite design techniques. The results confirm that the optimum shape of the airfoil is very close to the symmetrical shapes. Although these studies are instructive in choosing the blade profile for the VAWT, a more comprehensive study on the camber, the camber's location as well as the thickness of the VAWT is still very important.

Although 2D simulations afford many useful results for the design of the VAWT, it cannot reflect the 3D phenomenon that affects the blade's performances since the vortices caused by the trailing edge and the blade tip are always overlooked in these studies. Siddiqui et al.[16] found that the 2D simulation can over predict the performance by up to 32 percent in comparison with the real-time 3D CFD simulation because of the neglect of the 3D flow effects. In addition, 2D simulations are based on the assumption that the blade is straight and thus the influence of the blade's spanwise shape is still unknown. The influence of the tip vortex increases along the blade span towards the tip thus decreasing the power performance of the blade in comparison with the result obtained by a 2D assumption.[17] Bedon et al.'s[2] study shows that a changing chord length along the spanwise direction can improve the performance of the Troposkien geometry VAWT but only a few similar studies have been applied on the H-Darrieus type VAWT.

This paper numerically studies the influence of the blade's camber and the maximum camber's position on the performance of the VAWT using a 2D CFD approach. A Kriging model is established to find the optimal airfoil configuration to improve the power coefficient. Following this, the influence of the airfoil's thickness is also studied. Based on the results, we have studied the influence of the blade's spanwise configuration on the performance of the VAWT based on a 3D numerical approach. During this process, the rotor is simplified to a one blade model that rotates with the transient velocity and the attack angle conditions, which are acquired by the theoretical formulas. The results show that the straight blade with a symmetrical airfoil can improve the power efficiency under flow conditions simulated.

2. Modelling Strategy

In this paper, the two-blade VAWT model is used as shown in Figure 1, which is based on Li's experimental design.[12] The free stream wind speed is V_∞ flowing from the left-hand-side across the turbine. The rotor's rotation speed is ω and the rotor's radius and height are R and H, respectively. The tip speed ratio (TSR) is defined as $TSR = \omega R/V_\infty$.

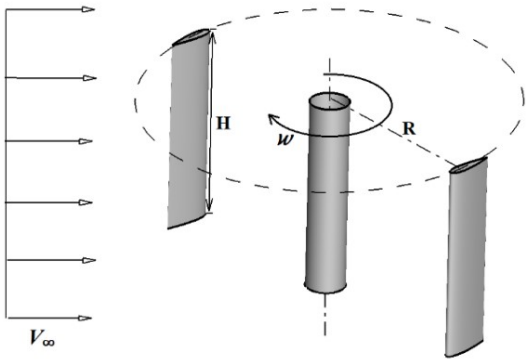

Figure 1: Schematic of the two-blade VAWT geometry.

When the rotor rotates, the relationship between the azimuthal angle (θ) and the blade attack angle (α) is given by

$$\alpha = \arctan\left(\frac{\sin\theta}{TSR + \cos\theta}\right) - \beta \tag{1}$$

where β is the pitching angle of the blade. The blade incident velocity can be calculated as follows

$$V_{real} = [\omega^2 R^2 + V_\infty^2 + 2\omega R V_\infty \cos\theta]^{1/2} \tag{2}$$

DOI: 10.13009/EUCASS2019-159

2.1 Physical models

This paper adopts both 2D and 3D simulations in studying the configuration of VAWT's blade. Based on the straight blade assumption, the 2D domain around the rotor is modelled using the sliding mesh approach. The airfoils are the NACA 4 digital series so that the thickness and the camber can be taken as the design variables. The 3D model has the same numerical settings as the 2D model but only one blade is considered in order to decrease the mesh size and save the computational cost.

2.1.1 Two dimensional model

Two blade model is applied in this simulation. The computational domain and boundary conditions of the model are shown in Figure 2. The slip wall condition on both sides of the domain is defined to avoid the influence of boundary layer. The velocity inlet have a turbulent intensity of 0.5% and a turbulent viscosity ratio of 10 and the free flow velocity is 8m/s. In order to simulate the rotation of the blade, a sliding mesh is adopted. As shown in Figure 2, the domain is divided into 3 parts by two interfaces. Both the outside part and the inner part are stationary. The ring shaped part together with the 2 blades rotate around the shaft's axis, and the rotation speed of this part is 17.52 rad/s. In this study, the blade's radius is 1m and the chord length of the blade is 0.265m and the tip speed ratio is 2.19. These conditions are based on the flow condition of Li's work[11] because the experimental data is available to compare with. In order to correctly reflect the flow character in the flow field, the rotor is placed 10 radius from the inlet and 25 radius from the outlet thus the domain is 20 radius wide.

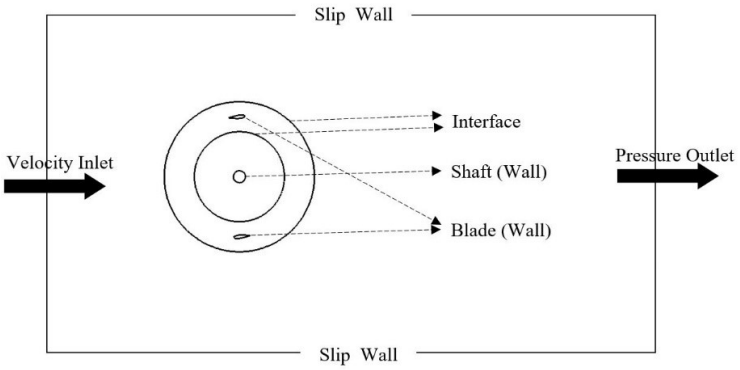

Figure 2: The computational domain and boundary conditions of the 2D model.

2.1.2 Three dimensional model

2 dimensional modelling process is efficient in studying the cross section shape of the blade. However, it cannot simulate the span wise flow. As a result, the blade's configuration in the span wise direction has to be studied using a 3 dimensional CFD approach. In this paper, the full scale VAWT model is simplified using a one blade model, which flaps around its center axis in the flow field. The free flow velocity and the angle of attack of the blade is defined as a function of the flow time based on equations (1) and (2). Since the blade is symmetrical up and down, then only half on the model is considered in the domain in order to reduce the computational cost. A similar numerical set up is reported in our previous publication[17] with more detailed descriptions. The chord length of the blade is c = 0.225m. The domain is 19c long and 13.2c wide with a height of 6.8c, which is also 3 times that of the half-blade's length(H, H = 0.51m). Except for the bottom surface being defined as the symmetry condition, the other three surfaces of the domain, parallel with the flow direction, are defined as the slip wall condition. In this 3D model, the free flow velocity is V_∞=7m/s and the TSR is 2.29 based on Li's experiment[12] so that the rotation speed is ω=18.86/s. This parameters can be employed in equation (1) and (2), in which $\theta = \omega \cdot t$ is used to calculate the transient α and V_{real}.

2.2 Meshing strategy

The geometry, as well as the mesh, in the flow field is generated using the design module in Ansys 18.2. In both the 2D and 3D simulations, the sliding mesh strategy is adopted but the mesh motions are controlled in different ways. Figure 3 shows the mesh in a 2D computation domain and the local mesh around the airfoil. We adopted hybrid grids for 2D domains and only the ring shaped part adopts un-structural grid while the other two parts adopt structural grid.

DOI: 10.13009/EUCASS2019-159

The grids are encrypted towards the surface of the airfoils(blade) and the shaft in order to capture the boundary layer around the wall and maintain a small y+ value. The grids are also encrypted in the wake region of the rotor so that the flow field characteristics can be captured in detail.

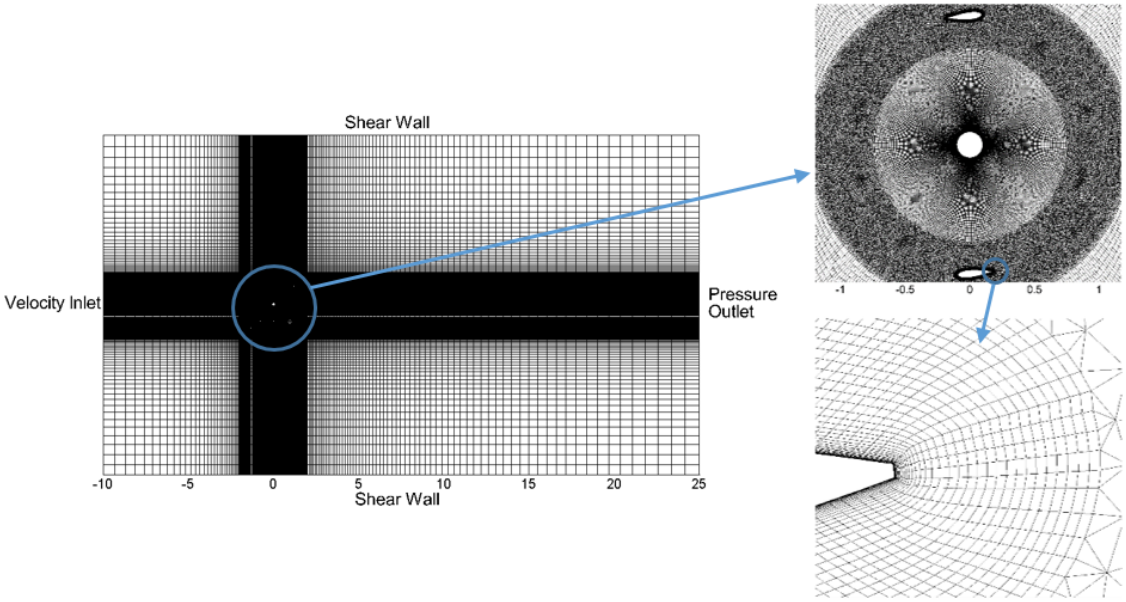

Figure 3: The mesh in 2D domain and the local mesh around the blade.

2.3 Grid independent analysis

In order to validate the 2D numerical model used in the simulation, 3 meshes with different grid scales are used, namely coarse mesh, medium mesh and refined mesh. The cell numbers of these meshes are listed in Table 1. The model uses NACA0021 as the blades' profile. The tip speed ratio is 2.19 and the flow condition is that introduced in Li's work.[11] The tangential coefficient versus azimuthal angle simulated by these grids are compared with the experimental data[11] (Shown in Figure 4). The figure shows that all these grids over predict the tangential coefficient of the blade in comparison with the experimental result and the reason for this is that the two-dimensional simulation cannot consider the tip vortex and other 3-D flow characteristics. The result is reasonable since the 2-D simulations in other literatures show the same phenomenon. The coarse grid shows greater inconsistencies with the experiment data in comparison with the other 2 grids. The medium grid and the refined grid matches well and both of them can reflect the basic characteristics as in the experiment data. As a result, this paper adopts the refined grid as the 2D simulation mesh.

Table 1: The 2D meshes used in the grid independent analysis.

Grid	**Coarse**	**Medium**	**Refined**
Cell No.	101288	131199	205582
Y+	<1	<1	<1

In addition, the 3D one blade model is also validated by the experimental data in Li's work.[12] In this simulation, a 2 blade VAWT with the NACA 0015 blade profile is utilized. The flow condition is shown in another Li's work.[12] The torque coefficient in the middle section of the blade as a function of the azimuthal angle is compared. Also we used the basic grid together with the coarse grid and the refined grid to conduct the grid independence analysis and the result in Figure 5 reflects that the basic grid and the refined grid produce similar result and all of the results obtained by these grids match well with the experimental data in the up-stroke region. Since the one blade model cannot consider the blade-blade flow interactions and the influence of the shaft on the blade's performance, the down-stroke results of the simulations differ substantially with the experimental data. However, the effective power generation is generated mainly by the up-stroke stage, thus this difference is assumed to be less influential on the final results. In addition, we have enlarged the flow field domain based on the basic grid and the result is shown as the red dashed line in Figure 5.

DOI: 10.13009/EUCASS2019-159

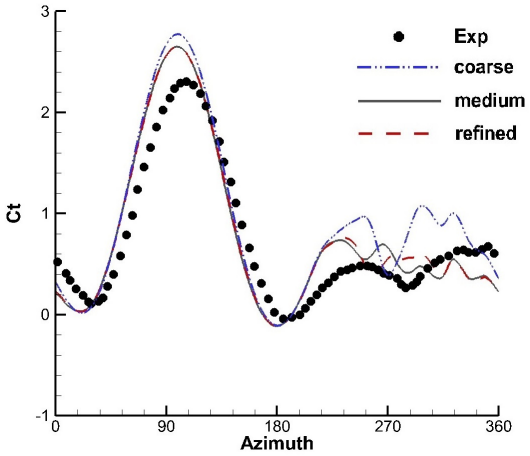

Figure 4: Comparison of the tangential coefficient on a VAWT blade for the 2D grid independence analysis.

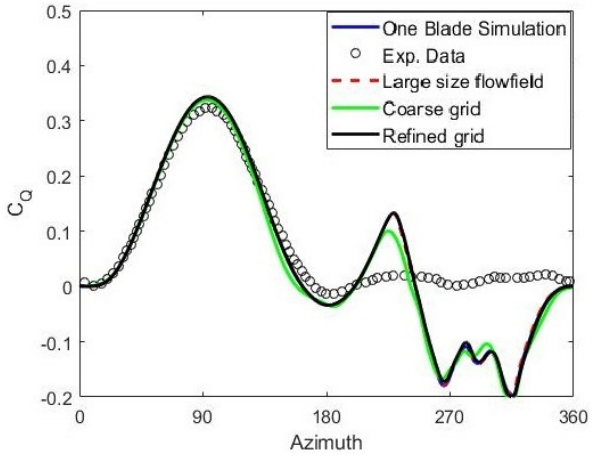

Figure 5: Comparison of the torque coefficient for the one-blade models and the experimental data.

It is clear that this result matches well with the basic grid with a smaller computational domain. As a result, the basic grid is used in the following 3D simulations.

2.4 Simulation strategy

The Reynolds-averaged Naviere-Stokes equations and the two equations transient SST $k-\omega$ turbulence model have been utilized to simulate the rotating process of both the 2D rotating models and the 3D pitching models. The double precision pressure based coupled solver algorithm is utilized in the transient mode and the second-order scheme is used for the spatial and temporal discretization. The SIMPLEC pressure-velocity coupling scheme with the second-order implicit transient formulation are adopted in the solver and the transient time step sizes are set to be 0.0005977s for the 2D model and 0.000555s for the 3D model so that the rotational angle per time step is 0.6°. The relative motion between the turbine and the absolute reference frame is modelled using a sliding mesh interface. In the 2D model, the ring part, as mentioned above, is a moving part, rotating with a speed 17.52 rad/s. In the 3D model, the mesh around the single blade is set to be the dynamic mesh, controlled by an UDF file to control its rotating speed. The changing free flow velocity is also controlled by the UDF file, applied on the velocity inlet. All the cases studied in the current work has a fixed pitching angle of 6° because such an arrangement has been proved to have a good performance.[11,12] The simulations are run on the high performance computer at Sheffield University, and each case employs 32 cores.

3. Problem definition

Firstly this paper studies the influence of the airfoil's camber and the maximum camber position on the performance of the rotor based on the 2D CFD approach. Based on the symmetrical airfoil, the thickness's influence is also studied. After that, we use the 3D CFD approach to study the shape of the blade along the span wise direction and investigate whether the straight blade is the best choice.

In this paper, the NACA 4 digital airfoil series is chosen because the definition is straight forward. Typical NACA 4 digital airfoil has the name *NACA MPXX*, where M is the value of the maximum camber divided by 100, P is the position of the maximum camber divided by 10, XX is the thickness of the airfoil divided by 100. Take NACA 1412 as an example, assuming that the chord length is 100, then this airfoil's thickness is 12 with a maximum camber of 1, which is located at the 40% of the chord.

In order to study the influence of the camber, the thickness of the airfoil is fixed and the two parameters, namely M and P, are used as the design variables in the 2D simulation. This paper adopts the Latin hypercube sampling approach to sample airfoils with different values of M and P. The power coefficients of the rotors with these airfoils are obtained so that the Kriging model is established. The Kriging model can reflect the best combination of M and P in improving the power coefficient.

After the camber's influence has been studied, we fixed the values of M and P to zero and studied the influence of the thickness (XX). In this process, the NACA 0006, 0012, 0015, 0018, 0021 and 0024 are chosen and a comparison of these airfoils are shown in Figure 6.

DOI: 10.13009/EUCASS2019-159

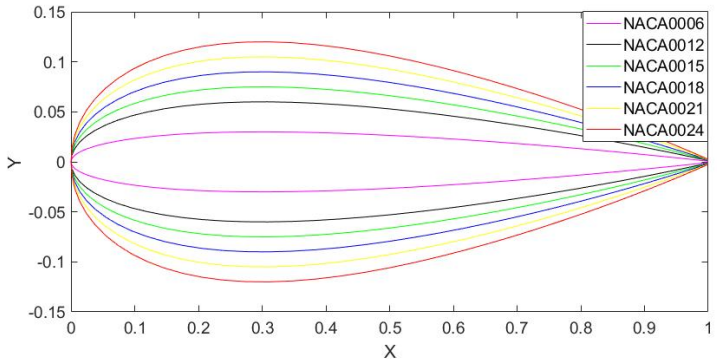

Figure 6: Comparison of the airfoils with different thickness.

Through 3D simulations, the influence of the blade's span wise shape has been studied. We used 6 different blades with the same sectional profile, namely NACA0015, and the same chord length in the symmetry plane. The straight blade, which is used in the grid independence analysis, is set to be the reference case. The side views of the other 5 blades are shown in Figure 7. As shown in this figure, these blades are named parallelogram-1 (Case a), parallelogram-2 (Case b), Trapezoidal-1 (Case c), Trapezoidal-2 (Case d) and Trapezoidal-3 (Case e), respectively. The chord length distribution laws along the span wise direction of Case c to Case e are different. The aim of this setting is to find out whether the changing chord length along the blade's span wise direction will change the vortices structure around the blade and improve the performance of the blade.

Figure 7: Comparison of the blades with different span wise shapes (a) parallelogram-1, (b) parallelogram-2, (c) Trapezoidal-1, (d) Trapezoidal-2, (e) Trapezoidal-3

4. Result and analysis

4.1 The influence of the airfoil's camber

In this section, both the camber and the maximum camber's position on the airfoil is studied, with the NACA0021 being the base airfoil. All the airfoils have the same thickness. As mentioned in the above section, M and P stand for the maximum camber and it's position, respectively, for the NACA 4 digital airfoils. We adopted the Kriging model to establish the surrogate relationship of the power coefficient as a function of M and P. The sampling process adopts the Latin hypercube sampling (LHS) approach.[20] The sampling of M ranges from -9 to 9 and the sampling of P ranges from 10 to 90 because these settings cover almost all the NACA 4 digital airfoil shapes at the given thickness. The sampling points, as well as the corresponding blades' power coefficients, are listed in Table 2. Based on the results, a Kriging model[19] is established based on the data and the results. In order to make the model more convincing, the adding-point approach based on the maximum mean square prediction errors (MSPE)[8,14] is adopted. This approach adds sampling points to where the MSPE value is too large. As a result, the final model results are shown in Figure 8. In this figure, the pink points are all the sampling points used in the establishing of the model. The black points and the blue points

DOI: 10.13009/EUCASS2019-159

are the validation points, which represents the predicted results and the actual results, respectively. Since the black points and the blue points match well, we can conclude that the model is precise enough. The red line in the figure is the predicted result for the non-camber airfoils in that the value of M is 0. The noted point, $[-0.36, 29.2, 0.2535]$, in this figure is the point with the maximum power coefficient. This figure shows that the airfoil with the maximum power coefficient is very close to the symmetrical airfoil and its maximum camber is only 0.36% of the chord length. Overall, the symmetrical airfoil has a better power coefficient performance than the cambered airfoils with the same thickness.

Table 2: Latin hypercube sampling points and the corresponding blades' power coefficients

No.	M	P	**Cp**
1	-3.11	26.22	0.2017
2	-0.63	85.02	0.2284
3	3.17	65.19	0.1921
4	6.19	37.32	0.0882
5	-3.96	55.18	0.2083
6	1.13	49.42	0.2164
7	6.91	74.74	0.1608
8	-8.96	33.48	0.0807
9	0.36	17.10	0.2295
10	-1.58	52.35	0.2418
11	-5.55	75.49	0.1969
12	-6.16	22.30	0.1075
13	4.24	42.84	0.1304
14	8.55	62.29	0.0908
15	-7.54	11.44	0.0487
16	5.00	84.92	0.2132

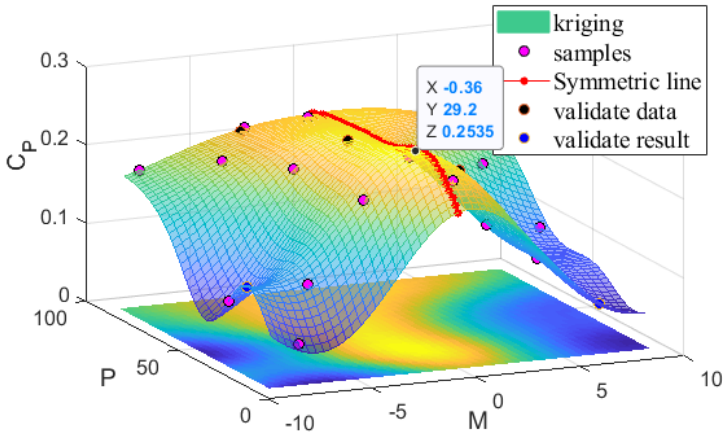

Figure 8: Kriging model of the power coefficient as a function of the maximum camber and its position.

4.2 The influence of the airfoil's thickness

Since the symmetrical airfoil has been proved to have a good performance in the above section, the thickness's influence on the symmetrical airfoi is studied in this section. We adopted six airfoils with different thickness, which are compared in Figure 6. The free flow condition and the settings in the numerical simulations are all the same for all the airfoils and the results are shown in Table 3 and Figure 9. The results show that with an increase in the thickness, the power coefficient increases to a maximum value before decreasing. The NACA0018 has the maximum power coefficient with a value of 0.2601 so that its performance is the best among all the six airfoils in the current flow condition. Figure 9 is the torque coefficient as a function of the azimuthal angle and the tick labels on the horizontal axis shows that it is obtained when the rotor is rotating at the 4th cycle. This figure shows that, apart from NACA0006, the torque

DOI: 10.13009/EUCASS2019-159

coefficient in the up-stroke stage decreases with an increase in the airfoil thickness. However, in the down-stroke stage, the NACA0018 airfoil performs the best so that the overall performance of the NACA0018 is the best.

Table 3: Power coefficients comparison among airfoils with different thickness.

Airfoil	**NACA0006**	**NACA0012**	**NACA0015**	**NACA0018**	**NACA0021**	**NACA0024**
Cp	0.0189	0.1279	0.2544	0.2601	0.2349	0.1961

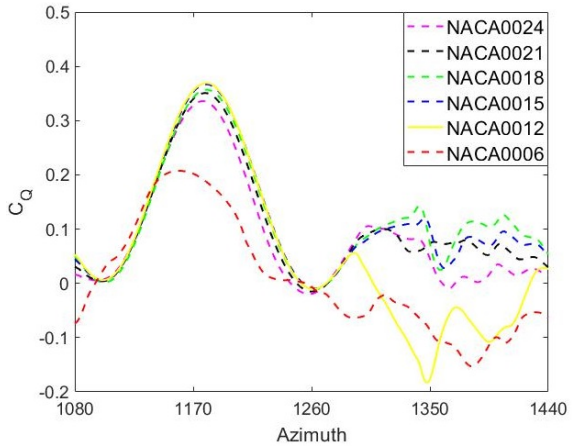

Figure 9: 2D VAWTs' torque coefficients comparison for the airfoils with different thickness.

Figure 9 shows that the NACA0006's torque pattern is very different from that in the other airfoils. This is because a fixed pitching angle of 6° makes the blade stall at the the start point since the stall limit angle of attack of the NACA0006 is very small. In addition, the blade stalls most of the time with the NACA0006 being the profile so that the overall performance is poor. In addition, the down-stroke performance of the NACA0012 is also very different from the thicker airfoils. That is also caused by the flow separation phenomenon since the flow around a thinner symmetric airfoil separates earlier than the thicker airfoils as the attack angle grows. Because of the fixed pitching angle in this study, the absolute value of the angle of attack in the down-stroke stage is larger than that in the up-stroke stage and the flow around the NACA 0012 airfoil separates in the down-stroke stage but not separates in the up-stroke stage. Figure 10 compares the contours of the turbulent kinetic energy for different blade profiles in three azimuthal positions. The detached vortexes shown in this figure reflect the flow separation during the corresponding azimuthal angles. This figure can reflect that the thicker the blade profile is, the less likely the flow separates during the rotation process. Overall, the NACA0018's thickness is the most suitable one in the current flow and operation condition.

Since the NACA0018 blade profile has slightly better power performance than the NACA0015 and the NACA0021 blade profiles at the TSR condition of 2.19, it is necessary to find out whether it perform the best at other TSR conditions. In this study, we also did the simulation at TSR conditions from 0.5 to 3.5 by changing the rotation speed of the rotors with different blade profiles. Figure 11 compares the power coefficients at TSR conditions from 0.5 to 3.5 for the NACA0015, the NACA0018 and the NACA0021 blade profiles. As can be seen in this figure, the NACA0015 blade profile has a lowest performance at low TSR conditions but highest power performance at high TSR conditions. On the contrast, the NACA0021 blade profile performs slightly better at low TSR conditions but worse at high TSR conditions. The NACA0018 blade profile, with a thickness between the NACA0015 profile and the NACA0021 profile has the best performance at the moderate TSR conditions around 2. As a result, the blade profile should be chosen by taking the rotor's working condition into consideration. For example, if the rotor normally works in a high TSR condition, blade profiles should be chosen from those thinner airfoils and vice versa.

4.3 The influence of the blade's span wise shape

In this section, the one-blade models with the NACA0021 being the blades' profile are used to study the influence of the span wise chord length distribution on the blades' performance. The torque coefficient as a function of the azimuthal angle is compared in Figure 12. The base blade is the straight blade that is commonly used in the practical applications. The base blade's power coefficient is 0.0917 while the other 5 blades' power coefficients are 0.0922, 0.0917, 0.0617, 0.0772, 0.0719 for the case (a)-(e), respectively. It shows that the blade with a uniform chord length along the span

DOI: 10.13009/EUCASS2019-159

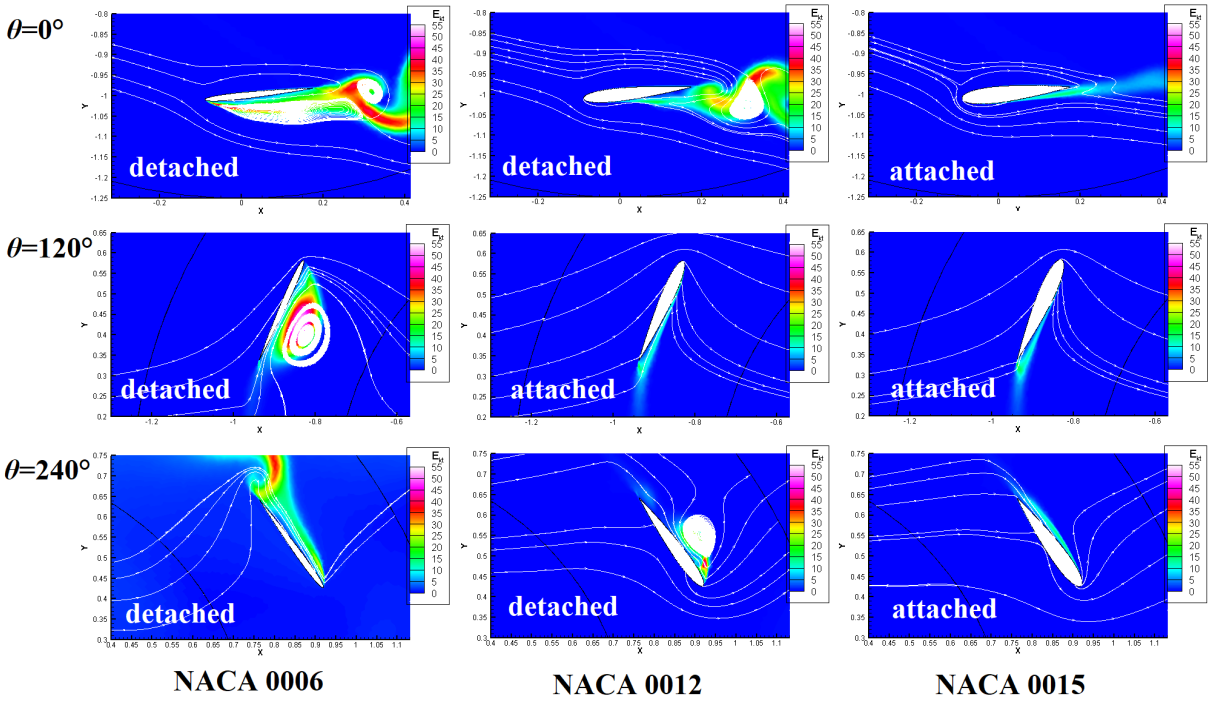

Figure 10: Contours of the turbulent kinetic energy for different blade profiles in three azimuthal positions.

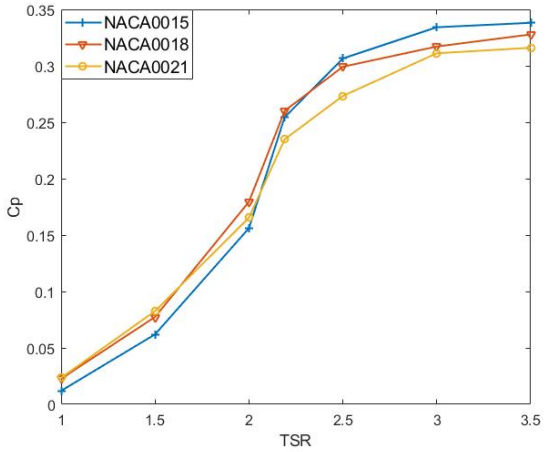

Figure 11: Comparison of power coefficients at different TSR conditions for 3 blade profiles.

DOI: 10.13009/EUCASS2019-159

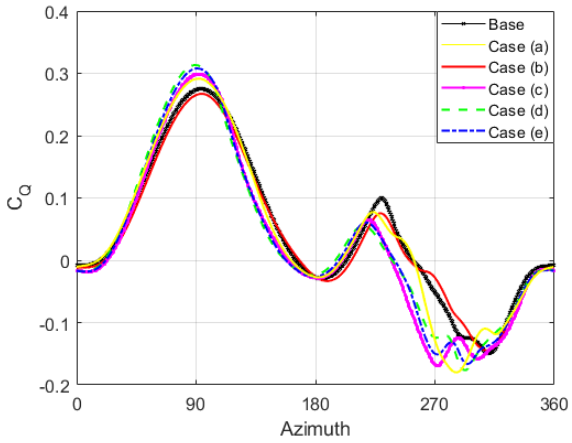

Figure 12: 3D VAWTs' torque coefficients comparison for the blades with different span wise shapes.

wise direction has a better performance than the trapezoidal blades with shorter chord length in the blade tip. Figure 12 shows that although most of the studied blades have higher maximum torque coefficient in the up-stroke part than the base blade, the torque coefficients reduce earlier and they perform worse in the down-stroke part. The reason why the trapezoidal blades have higher maximum torque coefficient can be explained by Figure 13. In this figure, all the contour snapshots are taken when the corresponding azimuthal angle is 90°. The streamlines, the pressure contours on the blades as well as the iso-surface contours for the Q-criterion level=0.005(The Q-criterion is a method to describe the instantaneous vortex structures, which reflects the 3D structures of the flow field[10]) are compared in this figure. It is clear that the tip vortices of the trapezoidal blades are smaller than those vortices of the blades with uniform chord length along the span wise direction. This phenomenon results in the good performance of the trapezoidal blades in this azimuthal angle. As a result, if the designers take more concern on the maximum torque of the blade, trapezoidal blades with shorter blade tip length are more attractive.

Case(a), which is a parallelogram blade with a back forward sweep angle, performs better than the straight blade but the improvement is moderate. In addition, the sweep angle of Case(a) is set to be 10° in the current study, therefore, the sweep angle's influence can also be studied in the future. Although the trapezoidal blades studied in this work has a less well performance than the straight blade, the influence of the other trapezoidal blades with longer chord length in the blade tip are also worthy of future study.

It should be noted that the single blade simulation adopted in this paper can only theoretically reflect the motion pattern of the VAWT blade but the real flow characteristics of them are different. The full turbine simulation will still be necessary to validate the performance of the blade.

5. Conclusion

This paper has used a 2D numerical model to study the influence of the camber and the thickness of the blade airfoil on the power coefficient performance of the VAWT. A 3D one blade model has been adopted to study the influence of the blade's span wise shape on the blade's performance. The conclusions are as follows:

(a) Symmetrical airfoils perform better than asymmetrical airfoils with the same thickness and under the same operation conditions.

(b) In the current study with a TSR value of 2.19 and a fixed pitching angle of 6°, the NACA0018 performs the best among all the six airfoils with different thickness that have been investigated. With the increase in the thickness that has been investigated, the power coefficient shows a trend of increasing first and then reducing.

(c) The trapezoidal blades with a shorter tip chord length than the central area perform better in the up-stroke stage than the parallelogram blades but their overall performance is less good.

The current study proves that the commonly adopted straight VAWT blade with symmetrical airfoils to be the profile is effective. The thickness of the blade and the sweep angle of it can be further optimized according to the predicted operational conditions.

DOI: 10.13009/EUCASS2019-159

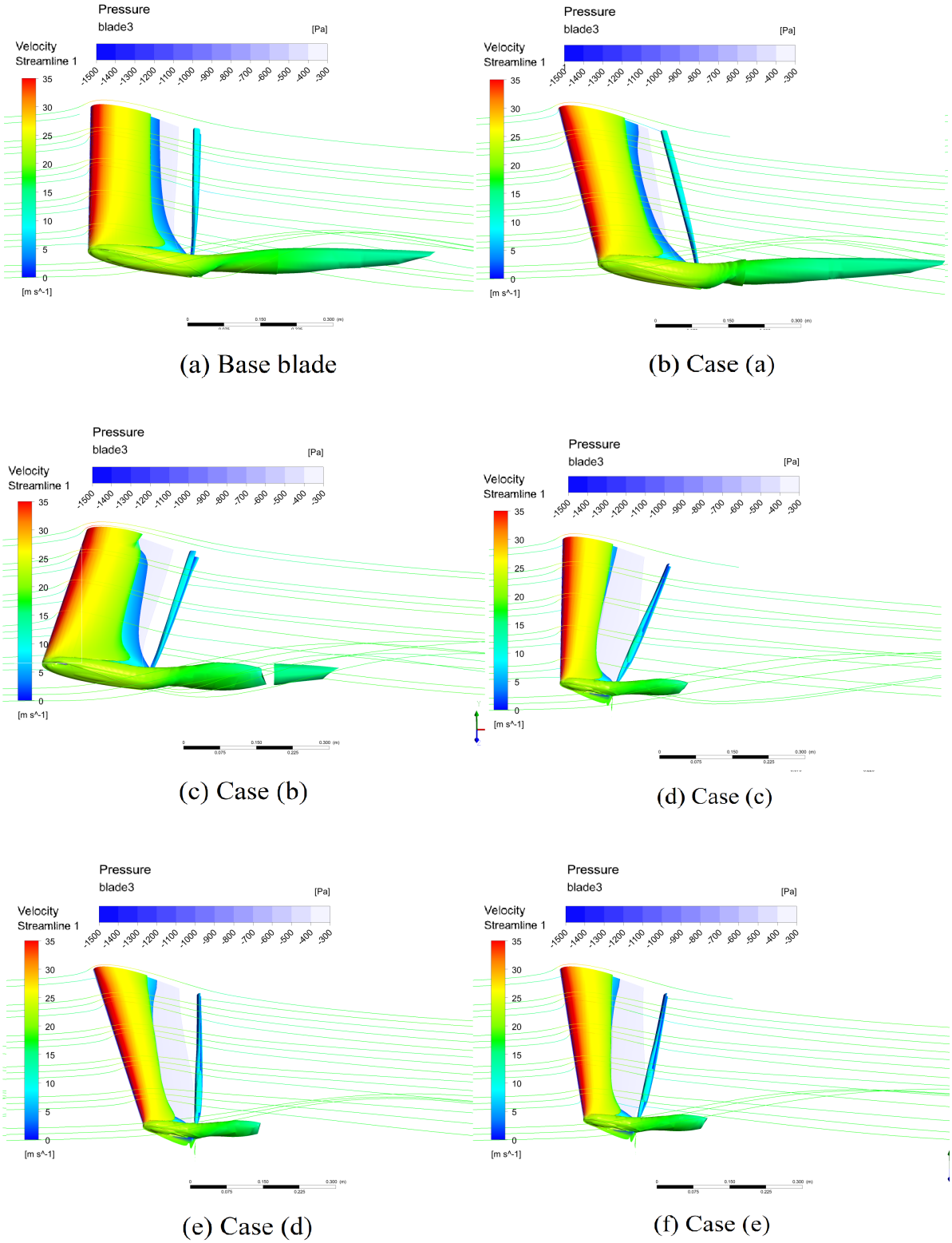

Figure 13: A comparison of the flow characteristics among the blades with different span wise shapes when the azimuthal angle is 90°.

6. Acknowledgments

Tiantian Zhang would like to acknowledge the China Scholarship Council and the University of Sheffield for funding his research studies. The authors also acknowledge the support from the National Natural Science Foundation of China

DOI: 10.13009/EUCASS2019-159

(Nos.11802340 and 11502291).

References

[1] Muhammad Mahmood Aslam Bhutta, Nasir Hayat, Ahmed Uzair Farooq, Zain Ali, Sh Rehan Jamil, and Zahid Hussain. Vertical axis wind turbine - a review of various configurations and design techniques. *Renewable and Sustainable Energy Reviews*, 16(4):1926–1939, 2012.

[2] Gabriele Bedon, Uwe Schmidt Paulsen, Helge Aagaard Madsen, Federico Belloni, Marco Raciti Castelli, and Ernesto Benini. Computational assessment of the deepwind aerodynamic performance with different blade and airfoil configurations. *Applied Energy*, 185:1100–1108, 2017.

[3] A. Bianchini, F. Balduzzi, J. M. Rainbird, J. Peiró, J. M. R. Graham, G. Ferrara, and L. Ferrari. On the influence of virtual camber effect on airfoil polars for use in simulations of darrieus wind turbines. *Energy Conversion and Management*, 106:373–384, 2015.

[4] S. Brusca, R. Lanzafame, and M. Messina. Design of a vertical-axis wind turbine: how the aspect ratio affects the turbine's performance. *International Journal of Energy and Environmental Engineering*, 5(4):333–340, 2014.

[5] J. Chen, L. Chen, H. Xu, H. Yang, C. Ye, and D. Liu. Performance improvement of a vertical axis wind turbine by comprehensive assessment of an airfoil family. *Energy*, 114:318–331, 2016.

[6] Fluent. *ANSYS. 18.2 User's Guide*. Ansys Inc., 2017.

[7] M. Jafaryar, R. Kamrani, M. Gorji-Bandpy, M. Hatami, and D. D. Ganji. Numerical optimization of the asymmetric blades mounted on a vertical axis cross-flow wind turbine. *International Communications in Heat and Mass Transfer*, 70:93–104, 2016.

[8] V. Roshan Joseph. Limit kriging. *Technometrics*, 48(4):458–466, 2006.

[9] Rosario Lanzafame, Stefano Mauro, and Michele Messina. 2d cfd modeling of h-darrieus wind turbines using a transition turbulence model. *Energy Procedia*, 45:131–140, 2014.

[10] H. Lei, D. Zhou, Y. Bao, Y. Li, and Z. Han. Three-dimensional improved delayed detached eddy simulation of a two-bladed vertical axis wind turbine. *Energy Conversion and Management*, 133:235–248, 2017.

[11] Q. Li, T. Maeda, Y. Kamada, J. Murata, K. Furukawa, and M. Yamamoto. Effect of number of blades on aerodynamic forces on a straight-bladed vertical axis wind turbine. *Energy*, 90:784–795, 2015.

[12] Qing'an Li, Takao Maeda, Yasunari Kamada, Junsuke Murata, Toshiaki Kawabata, Kento Shimizu, Tatsuhiko Ogasawara, Alisa Nakai, and Takuji Kasuya. Wind tunnel and numerical study of a straight-bladed vertical axis wind turbine in three-dimensional analysis (part i: For predicting aerodynamic loads and performance). *Energy*, 106:443–452, 2016.

[13] D. MacPhee and A. Beyene. Recent advances in rotor design of vertical axis wind turbines. *Wind Engineering*, 36(6):647–666, 2012.

[14] Markus P. Rumpfkeil and Philip Beran. Construction of dynamic multifidelity locally optimized surrogate models. *AIAA Journal*, 2017.

[15] D. L. Shukla, A. U. Mehta, and K. V. Modi. Dynamic overset 2d cfd numerical simulation of a small vertical axis wind turbine. *International Journal of Ambient Energy*, 2018.

[16] M. S. Siddiqui, N. Durrani, and I. Akhtar. Quantification of the effects of geometric approximations on the performance of a vertical axis wind turbine. *Renewable Energy*, 74:661–670, 2015.

[17] Tian tian Zhang, Mohamed Elsakka, Wei Huang, Zhen guo Wang, Derek B. Ingham, Lin Ma, and Mohamed Pourkashanian. Winglet design for vertical axis wind turbines based on a design of experiment and cfd approach. *Energy Conversion and Management*, 195:712 – 726, 2019.

[18] A. Tummala, R. K. Velamati, D. K. Sinha, V. Indraja, and V. H. Krishna. A review on small scale wind turbines. *Renewable and Sustainable Energy Reviews*, 56:1351–1371, 2016.

DOI: 10.13009/EUCASS2019-159

[19] Raul Yondo, Esther Andrés, and Eusebio Valero. A review on design of experiments and surrogate models in aircraft real-time and many-query aerodynamic analyses. *Progress in Aerospace Sciences*, 96:23–61, 2018.

[20] Tian-tian Zhang, Wei Huang, Zhen-guo Wang, and Li Yan. A study of airfoil parameterization, modeling, and optimization based on the computational fluid dynamics method. *Journal of Zhejiang University-SCIENCE A (Applied Physics & Engineering)*, 17(8):632–645, 2016.